

A new lidar inversion method using a surface reference target. Application to the backscattering coefficient and lidar ratio retrievals of a fog-oil plume at short-range

Florian Gaudfrin^{1,2,3}, Olivier Pujol², Romain Ceolato¹, Guillaume Huss³, and Nicolas Riviere¹

¹ONERA / DOTA, Université de Toulouse, F-31055 Toulouse - France

²Université de Lille, Département de physique, Laboratoire d'optique atmosphérique, 59655 Villeneuve d'Ascq, France

³LEUKOS, 37 rue Henri Giffard, 87280 Limoges, France

Correspondence: Florian Gaudfrin (florian.gaudfrin@onera.fr)

Abstract. In this paper, a new elastic lidar inversion equation is presented. It is based on the backscattering signal from a surface reference target (SRT) rather than that from a volumetric layer of reference (Rayleigh molecular scatterer) as usually done. The method presented can be used when the optical properties of such a layer are not available, *e.g.* in the case of airborne elastic lidar measurements or when the lidar-target line is horizontal. Also, a new algorithm is described to retrieve the lidar ratio and the backscattering coefficient of an aerosol plume without any *a priori* assumptions about the plume. In addition, our algorithm allows a determination of the instrumental constant. This algorithm is theoretically tested, *viz.* by means of simulated lidar profiles, and then using real measurements. Good agreement with available data in the literature has been found.

Copyright statement.

1 Introduction

Atmospheric aerosols are liquid or solid particles dispersed in the air (Glickman and Zenk, 2000) of natural (volcano, biomass burnings, desert, ocean) or anthropogenic origins. They play an important role in cloud formation (DeMott et al., 2010), radiative forcing (Hansen et al., 1997)(Hay, 2000) and more generally for researches on the climate change, but also in the context of air quality and public health (Bal, 2008; Finlayson-Pitts and Pitts, 2000; Popovicheva et al., 2019; Zhang et al., 2018). Their size varies from the nanometer to the millimeter scale (Robert, n.d.). However, a large majority of aerosols have a size between $0.01 \mu\text{m}$ and $3 \mu\text{m}$ (Clark and Whitby, 1967) for which scattering is dominant in the optical domain. The Mie theory is often used, at least statistically (*i.e.* for a large population of random sized aerosols), although aerosols are not always spherical. The optical backscattering and extinction properties of aerosols are mainly related to their shape (Ceolato et al., 2018), size distribution (Vargas-Ubera et al., 2007), concentration and chemical composition which is based to their nature (dust, maritime, urban). Lidar are active remote sensing instruments suitable for aerosol detection and characterization (Sicard et al., 2002) over kilometric distances during both day and nighttime.

The optical properties of aerosols are obtained by means of inversion methods using the simple scattering lidar equation. In the 1980s, a stable one-component formulation adapted to lidar applications was proposed by Klett (1981). It has then been extended to a two-component formulation, *viz.* separating molecular and aerosol contributions, by Fernald (1984) and Klett (1985). The elastic lidar equation is an ill-posed problem in the sense of Hadamard (1908) since one searches for extinction and for backscattering coefficients with only a single observable. Several assumptions are therefore required in order to invert the lidar equation:

- (i) A calibration constant is usually determined from a volumetric layer of the upper atmosphere as a reference target (Vande Hey, 2014). This calibration layer can be very high in altitude; it has recently been moved from the around (32km) to around (36 – 39km) for the CALIPSO spaceborne lidar in order to reduce uncertainties in the inversion procedure (Kar et al., 2018; Getzewich et al., 2018). This volume is considered made only of pure molecular constituents whose optical scattering properties are well-known (Rayleigh regime). The molecular backscattering coefficient is generally estimated from the standard model of the atmosphere (Anon, 1976; Bodhaine et al., 1999). However, poor estimates of the reference or low signal-to-noise ratios (*SNR*) can lead to severe uncertainties on the retrieved extinction and backscattering coefficients. Few sensitivity studies have been performed to evaluate such uncertainties (Matsumoto and Takeuchi, 1994; Rocadenbosch et al., 2012). Spatial averaging around the volume of reference in addition to time averaging is thus recommended to increase *SNR*.
- (ii) Lidar ratio is constant over the distance range of measurements (Sasano et al., 1985). This is also a source of important errors in the retrieval values. Some studies have proposed a variable lidar ratio under the form of a power-law relationship between the extinction and backscattering coefficients, but such a method requires an *a priori* knowledge of the medium under study (Klett, 1985).
- (iii) The molecular contribution along the lidar-line is known. It is estimated, as for the backscattering coefficient, by means of temperature and pressure vertical profiles, using either the standard model of the atmosphere or radio soundings (Jäger, 2005).

In the case of elastic lidar inversion, the most critical parameter is the lidar ratio (*LR*). It depends on the wavelength (in vacuum) and on the microphysics, morphology, and size of the particles (Hoff et al., 2008). The *LR* ranges from 20sr to 100sr at 532nm (Ackermann, 1998; Cat, 2005; Leblanc et al., 2005) according to the aerosol origins (maritime, urban, dust particles, biomass burning). It is therefore difficult to assume an *a priori* value for *LR* in as much this information is to be found rather than given.

Several alternatives have been analyzed to constrain the inversion procedure while relaxing assumption (ii). These alternatives are based on the determination of the optical thickness, the one which consists in coupling lidar and sunphotometer measurements being the most largely used. The measured optical thickness is then used to constrain extinction profiles (Fernald et al., 1972; Pedrós et al., 2010). A second alternative, consists in combining elastic lidar and Raman measurements in order to get the optical depth as a function of range (Ansmann et al., 1990, 1992, 1997; Mattis et al., 2004). In a third technique, the

optical depth is retrieved from elastic lidar measurements with different zenith angles (Sicard et al., 2002). It is worth indicating that coupling lidar and sunphotometer measurements is possible only daytime while Raman measurements are carried out preferentially at nighttime in order to increase the SNR . A fourth method consists in the determination of the optical thickness and lidar ratio of transparent layers located above opaque clouds (Hu et al., 2007; Young, 1995) that are used as reference for calibration in the inversion procedure (O'Connor et al., 2004). This method is used for downlooking lidar measurements capable of measuring depolarization ratios. However, the method is limited to lidar systems in non-polarized detection and for lidar measurements for which clouds cannot be used as a reference. A fifth approach consists in the determination of the optical thickness of the atmosphere from the sea surface echo by combining lidar and radar measurements (Josset et al., 2010a, b, 2008). This method has been used to find the lidar ratio and the optical depth of aerosol layers over oceans (Dawson et al., 2015; Josset et al., 2012; Painemal et al., 2019).

Another limitation of ground-based lidar measurements is related to the overlap function that strongly impacts (and prevents) observation close to the instrument, *i.e.* in the lowest layers of the troposphere where aerosols are emitted. Different studies have proposed to modify the overlap function analytically (Comeron et al., 2011; Halldórsson and Langerholc, 1978; Kumar and Rocadenbosch, 2013; Stelmaszczyk et al., 2005) or empirically (Vande Hey et al., 2011; Wandinger and Ansmann, 2002). Some lidar devices are also equipped with a second telescope of higher overlap at short range (Ansmann et al., 2001). However, current lidar systems are not adapted enough to the monitoring and characterization of volumetric targets at short-range, for instance in the industrial context, or more generally, for anthropogenic activities (Ceolato and Gaudfrin, 2018).

To meet new industrial emission control requirements and very recently emitted anthropogenic aerosols characterization, we have developed a short-range lidar of high spatial resolution (Gaudfrin et al., 2019)(Gaudfrin et al., 2018b). The lidar inversion cannot be performed by means of the classical Klett-Fernald equation, because the reference layer used for the inversion is either impossible to access (horizontal lidar measurements, sky-to-ground lidar airborne measurements), or inaccessible because of finite lidar range. In the present paper, a modification of the conventional lidar equation is proposed in order to perform lidar inversions using a surface reference target (SRT) at relatively short range ($r_{max} \approx 100$ m). Precisely, a unified lidar equation for surface and volumetric scattering media is suggested, and it is then used for a new inversion equation, inspired from the Klett-Fernald equation, using a SRT.

Also a new technique to retrieve the lidar ratio without using any sunphotometer, Raman or radar measurements is presented and applied to an aerosol plume. This new inversion technique is both assessed theoretically and experimentally using real lidar measurements. A discussion and a conclusion follow and close the present paper.

2 Unified lidar equation for surface and volumetric scattering media

Currently, lidar inversion methods use a volumetric layer of the upper atmosphere (higher than 8 km of altitude above ground level) as a reference target. This volume is considered as being free of aerosols and made only of pure molecular constituents whose optical scattering properties are known. In our approach, we propose to use a SRT of known bidirectional reflectance distribution function (BRDF) $f_{r,\lambda}$ (in sr^{-1}) (Nicodemus, 1965; Kavaya et al., 1983).

This requires to modify the usual lidar equation to make it suitable for both surface and volumetric targets.

For the single-scattering lidar equation, for which light has undergone only one scattering event, the measured backscattered power, at range r , can be written in a general way, *viz.* by considering both a surface target (Bufton, 1989; Hall and Ageno, 1970) and a volumetric target (Collis and Russell, 1976), as:

$$\mathcal{P}_\lambda(r, \theta_i) = \mathcal{P}_{p,\lambda} \frac{c\tau_\lambda}{2} \frac{A_{ef}}{r^2} \left\{ \beta_\lambda(r) + \frac{2}{c\tau_\lambda} f_{r,\lambda}(r_s, \theta_i) F_{cor} \right\} T_\lambda^2(r) \xi_\lambda(r) \eta_\lambda \quad (1)$$

where $\mathcal{P}_{p,\lambda}$ (in W) is the peak power of the laser source, $c \approx 3 \times 10^8 \text{ m} \cdot \text{s}^{-1}$ the Einstein's constant, τ_λ (in s) the laser pulse duration (full width at half maximum), A_{ef} (in m^2) the telescope effective receiving area θ_i (in rad) the angle between the normal eigenvector to the SRT and the incident beam direction. It should be noted that in the particular case of a Lambertian surface $f_{r,\lambda}(r_s, \theta_i)$ can be easily expressed by spectral bidirectional reflectance factor ρ_λ from $\rho_\lambda \cos \theta_i / \pi$ (Josset et al., 2018, 2010b; Haner et al., 1998). However, the general form of BRDF ($f_{r,\lambda}$) will be considered later in this work in order to not restrict the approach to specific cases. Also, the SRT is located at range r_s , ξ_λ the dimensionless overlap function, η_λ the dimensionless optical efficiency of the whole receiver. $\mathcal{P}_{p,\lambda}$ is a rectangular-shaped pulse in volumic lidar equation (Measures, 1992), *viz.* the ratio between the pulse energy and τ_λ . In the case of lidar measurements on a SRT, the backscattered peak-power is not proportional to $\mathcal{P}_{p,\lambda}$. A corrective factor F_{cor} depending on the real shape of the laser pulse is thus introduced. In the present case: $\mathcal{P}_{p,\lambda}^G = \mathcal{P}_{p,\lambda}^s F_{cor}$, with $\mathcal{P}_{p,\lambda}^G$ and $\mathcal{P}_{p,\lambda}^s$ the peak power of a Gaussian-shaped and a square laser pulse, respectively. Conservation of the pulse energy between these two kind of pulses gives $F_{cor} = 2(\ln 2 / \pi)^{1/2}$ (Paschotta, 2008). The factor does not apply to the volume part of the lidar equation because, in this last part, the pulse profile is assumed to be constant over a rate duration τ_λ . This approximation cannot be made on the backscatter peak of a SRT, because the backscattered energy is not integrated over a volume.

In Eq.1, T_λ^2 the back and forth atmospheric transmission throughout the environment between the lidar source and range r (Swinehart, 1962):

$$T_\lambda(r) = \exp \left[- \int_0^r \alpha_\lambda(x) dx \right] \quad (2)$$

α_λ (in m^{-1}) being the total extinction coefficient at wavelength λ , and range r : $\alpha_\lambda = \alpha_{b,\lambda} + \alpha_{a,\lambda}$. The subscripts "b" and "a" refer, respectively, to the contribution of the background (molecules, aerosols) and to the contribution of the aerosol volumetric target under investigation. The total backscattering coefficient β (in $\text{m}^{-1} \cdot \text{sr}^{-1}$) is $\beta_\lambda = \beta_{b,\lambda} + \beta_{a,\lambda}$, with the same meaning as just above for the subscripts. By definition, the corresponding lidar ratios are $LR_{b,\lambda}(r) = \alpha_{b,\lambda} / \beta_{b,\lambda}$ and $LR_{a,\lambda}(r) = \alpha_{a,\lambda} / \beta_{a,\lambda}$, respectively.

The fundamental quantity measured by the lidar instrument is a voltage V (in volts) which is proportionnal to the backscattered power: $V_\lambda(r) = R_{v,\lambda} \mathcal{P}_\lambda(r)$, where $R_{v,\lambda}$ is the detection constant (in $\text{V} \cdot \text{W}^{-1}$) which determines the light-voltage conversion. It can be written using the instrumental constant: $C_{ins} = R_{v,\lambda} K_s$ (in $\text{V} \cdot \text{m}^3$), where $K_s = \mathcal{P}_{p,\lambda} c \tau_\lambda A_{ef} \eta / 2$. In the literature, C_{ins} is obtained from \mathcal{P}_λ while, herein, it comes from the voltage and therefore takes into account all the emission, collection, detection and acquisition chain.

In the sequel, for better readability, the subscript λ and θ_i will not be written thereafter.

120 The range corrected lidar signal $V_\lambda(r)r^2$ is so:

$$S(r) = C_{ins} \left(\beta_a(r) + \beta_b(r) + f_r \frac{2}{c\tau} F_{cor} \right) \exp \left\{ -2 \int_0^r [\alpha_a(x) + \alpha_b(x)] dx \right\} \quad (3)$$

To remove the α -dependence in the exponential term, we will replace α_a and α_b by LR_a and LR_b , respectively, and introduce the term:

$$LR_a(r) \exp \left\{ -2 \int_0^r \beta_b(x) [LR_a(x) - LR_b(x)] dx \right\} \quad (4)$$

125 as detailed in Ansmann and Müller (2004). With such modifications, the final lidar equation for surface and volumetric scatterers can thus be written as:

$$S(r) LR_a(r) \exp \left\{ -2 \int_0^r \beta_b(x) [LR_a(x) - LR_b(x)] dx \right\} = C_{ins} \left[Y(r) + LR_a(r) \frac{2f_r}{c\tau} F_{cor} \right] \exp \left[-2 \int_0^r Y(x) dx \right] \quad (5)$$

with $Y(r) = LR_a(r) [\beta_b(r) + \beta_a(r)]$.

Thereafter, in order to highlight the expression to solve, it is convenient to define background corrected transmission factor:

$$130 \quad D(0, r) = \exp \left\{ -2 \int_0^r \beta_b(x) [LR_a(x) - LR_b(x)] dx \right\} \quad (6)$$

and $W(r) = S(r) LR_a(r) D(r)$. Finally, Eq. 3 becomes:

$$W(r) = C_{ins} \left[Y(r) + LR_a(r) \frac{2f_r}{c\tau} F_{cor} \right] \exp \left[-2 \int_0^r Y(x) dx \right] \quad (7)$$

We will now introduce the lidar framework adapted to the radiative parameter retrieval of a volumetric scattering medium with a known SRT.

135 3 New lidar inversion technique

3.1 Radiative parameters identification

The current Klett-Fernald inversion method consists in determining C_{ins} using the high atmosphere as a reference and to fix the LR_a a priori. In this paper, C_{ins} is determined by means of a SRT located at range r_s . So:

$$C_{ins} = \frac{c\tau}{2f_r F_{cor}} W(r_s) \frac{1}{LR_a(r_s)} \exp \left[2 \int_0^{r_s} Y(x) dx \right] \quad (8)$$

140 It is worth mentioning that $LR_a(r_s)$ is the lidar ratio just before the SRT and $Y(r_s) = 0$ (only at the SRT). Also, obviously, for $r < r_s$, $f_r = 0$. Inserting Eq. 8 in Eq. 7 gives:

$$W(r) = \frac{c\tau}{2f_r F_{cor}} \frac{W(r_s)}{LR_a(r_s)} Y(r) \exp \left[2 \int_r^{r_s} Y(x) dx \right] \quad (9)$$

This equation applies only before the SRT and can be solved by integrating both sides from r to r_s (Vande Hey, 2014). The exponential term is (see Appendix):

$$145 \exp \left[2 \int_r^{r_s} Y(x) dx \right] = 1 + \frac{4f_r F_{cor} LR_a(r_s)}{c\tau W(r_s)} \int_r^{r_s} W(x) dx \quad (10)$$

Plugging Eq. 10 into Eq. 9, we obtain in the following:

$$Y(r) = W(r) \left[\frac{c\tau W(r_s)}{2f_r F_{cor} LR_a(r_s)} + 2 \int_r^{r_s} W(x) dx \right]^{-1} \quad (11)$$

Using the definitions of $Y(r)$ and $W(r)$ (see above), $\beta_a(r)$ can be written as:

$$\beta_a(r) = S(r)D(0,r) \left[\frac{c\tau S(r_s)D(0,r_s)}{2f_r F_{cor}} + 2 \int_r^{r_s} S(x)LR_a(x)D(0,x) dx \right]^{-1} - \beta_b(r) \quad (12)$$

150 Multiplying the numerator and the denominator of the first term on the right-hand side of the subtraction by $D(r_s,0)$, this expression becomes:

$$\beta_a(r) = S(r)D(r_s,r) \left[\frac{c\tau S(r_s)}{2f_r F_{cor}} + 2 \int_r^{r_s} S(x)LR_a(x)D(r_s,x) dx \right]^{-1} - \beta_b(r) \quad (13)$$

Then, by definition of the lidar ratio, we deduct $\alpha_a(r) = LR_a(r)\beta_a(r)$. Eq. 13 is similar to the one defined by Klett (1981), except that β_b in Eq. 13 contains also the contribution of the aerosol background.

155 Assuming that the properties of the SRT are well known, the most critical parameter is $LR_a(r)$. Giving a value for LR_a requires an *a priori* knowledge of the volumetric target under study whereas the main objective of lidar remote sensing is precisely to characterize the medium investigated. *A priori*s are always topic of discussions and are more or less severe flaws in lidar measurements.

Equation 13 can also be applied on the important context of airborne observations. In this case, it is necessary to know the
160 ground *BRDF*.

3.2 Determination of LR_a and β_a : methodology

The objective is to retrieve first $\beta_a(r)$ and LR_a (and then to deduce $\alpha_a(r)$) without any *a priori* about the medium considered. Two lidar measurements are performed: the first one (signal V_s) in the absence of the volumetric aerosol medium of interest

and a subsequent one (signal V_{sv}) in its presence. The SRT is obviously present for both measurements. The two measurements
 165 should be performed close in time in order to avoid that the background environment evolves too much. The experimental setup
 of these lidar measurements is illustrated on Fig. 1

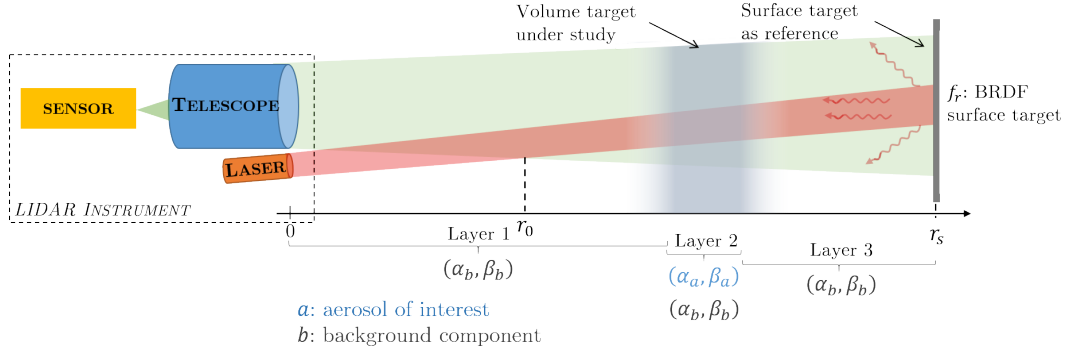


Figure 1. Illustration of the experimental setup

By definition, the half-logarithmic ratio of S_s and S_{sv} corresponds to the total extinction of the volumetric media under study: $\alpha_{tot} = \ln[S_s(r_s)/S_{sv}(r_s)]/2$. Using S_s , C_{ins} can be determined independently of the volumetric medium of interest:

$$C_{ins} = \frac{c\tau}{2f_r F_{cor}} S_s(r_s) \exp \left[2 \int_0^{r_s} \alpha_b(x) dx \right] \quad (14)$$

170 which is Eq. 8 with $\alpha_a = 0$. C_{ins} and α_{tot} are used in objective functions to retrieve LR_a , assumed to be uniform – r –independent. The first objective function is:

$$\varepsilon_1 = \left| \int_{r_0}^{r_s} \alpha_a(x) dx - \alpha_{tot} \right| \quad (15)$$

where α_a is the retrieved profile of extinction using Eq. 13 and LR_a . The medium is assumed to be at range of full overlap ($r > r_0$), so that α_{tot} must correspond to the integrated extinction. A second objective function:

$$175 \quad \varepsilon_2 = \left| \int_{r_0}^{r_s} [S_{sv}(x) - S_{sim}(x)] dx \right| \quad (16)$$

is introduced in order to minimize the difference between S_{sv} and the simulated signal S_{sim} obtained from the retrieved β_a and α_a and from C_{ins} .

The methodology is presented on Fig. 2. The molecular background contribution is computed from pressure and temperature data as in Bucholtz (1995), while the aerosol background contribution is estimated by means of radiative transfer codes, e.g.
 180 MATISSE (Simoneau et al., 2002; Labarre et al., 2010) or MODTRAN (Berk et al., 2008, 2014). Another solution consists in

using a realistic value of the visibility \mathcal{V} (in km^{-1}) and the Koschmieder's relation (Horvath, 1971; Elias et al., 2009; Hyslop, 2009) at 550 nm (maximum human eye sensitivity): $\mathcal{V}\alpha_b \approx 3.9$

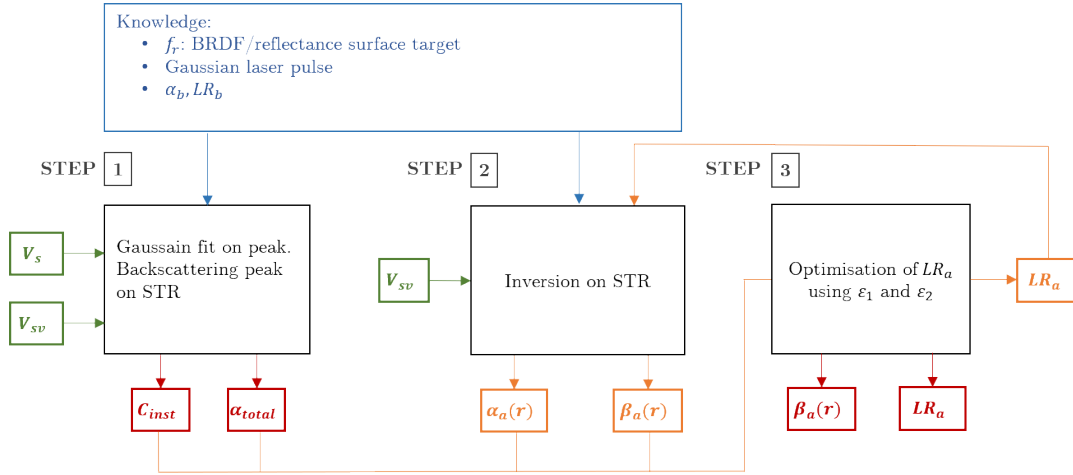


Figure 2. Diagram illustrating how the inversion algorithm allows to retrieve the $\beta_a(r)$ and LR_a without assumptions on the volume medium of interest. In green the lidar signals inputs, in orange the intermediate calculations during the optimization procedure and in red the code outputs.

The signals V_s and V_{sv} are introduced in the inversion procedure, which is organized around three main steps (Fig. 2):

1. A Gaussian fit is first applied on the backscattered signal from the SRT, *i.e.* $V_s(r_s)$ and $V_{sv}(r_s)$, that gives the amplitude of the backscattering, the position of this peak and its width in position. From these gaussian models, one can obtain α_{tot} (from its definition, see above) and C_{inst} from Eq. 14. Note: When the target is tilted with respect to the lidar-target line, the backscatter peak of surface target will not be symmetrical. An other fit should be used as a log-normal function.
2. A first lidar inversion is realized using Eq. 13 with $LR_a = 50\text{sr}$ at the beginning of the inversion procedure. This value has been chosen because it corresponds to the average LR_a data of the literature. For that, the gaussian model V_{sv} obtained at step 1 is used for signal $S(r_s)$ in Eq. 13. A first range-profile $\beta_a(r)$ is thus obtained at the end of this second step.
3. The above $\beta_a(r)$ and LR_a allow to determine $\alpha_a(r)$ whose r -integration is then compared with α_{tot} in the minimization procedure of Eq. 15. At each iteration, the LR_a is modified in order to reduce ϵ_1 . The new $\beta_a(r)$, LR_a , and so $\alpha_a(r)$ are then used to compute a simulated lidar signal S_{sim} whose comparison with S_{sv} is minimized according to Eq. 16. In this algorithm, the iterative procedure ends up when $\epsilon_1 + \epsilon_2 \leq 10^{-6}$ is reached. A number of 19 iterations is generally enough, depending on the first value of LR_a introduced initially (step 2). At the end of this step, one thus obtains final $\beta_a(r)$, $\alpha_a(r)$ and LR_a . The minimization procedure used is the one implemented by Kraft (1988). Eq. 15 is the most important since it determines the rapidity of convergence. Eq. 16 is helpful but not critical.

4 Theoretical behavior of the retrieval procedure

200 4.1 Theoretical lidar signals

The inversion method described above is tested using theoretical lidar signals generated by PERFALIS¹ (Gaudfrin et al., 2018a). As summarized in Table 1, the simulated atmosphere is composed of three layers and of a SRT of BRDF $f_r = 0.20/\pi$ located at $r_s = 100\text{m}$. Pressure and temperature are uniform (1040hPa and 290K) and the continental aerosol background is chosen so that it corresponds to $\mathcal{V} = 47\text{km}$ (Hess et al., 1998). In addition, $\beta_b = 1.05 \times 10^{-5} \text{m}^{-1} \cdot \text{sr}^{-1}$ and $LR_b = 51.01\text{sr}$. The signal V_s is generated from the background components and the SRT, while the signal V_{sv} is generated considering an aerosol plume aerosol between 20 – 30m (second layer). The plume backscatter coefficient is $\beta_a = 7.14 \times 10^{-5} \text{m}^{-1} \cdot \text{sr}^{-1}$ and $LR_a = 70\text{sr}$. Multiple scattering is assumed to be negligible. For dense atmosphere and wider field of view, Eq. 1 has to be corrected by an appropriate factor (Bissonnette, 1996) in order to consider higher orders of scattering events.

	Notation	Layer 1	Layer 2	Layer 3	SRT ($f_r = 0.20/\pi \text{sr}^{-1}$)
Range	r (in m)	0 – 20	20 – 30	30 – 100	100
Background components	α_b (in m^{-1})	1.18×10^{-3}	1.18×10^{-3}	1.18×10^{-3}	X
	β_b (in $\text{m}^{-1} \cdot \text{sr}^{-1}$)	9.97×10^{-6}	9.97×10^{-6}	9.97×10^{-6}	
	LR_b (in sr)	118.56	118.56	118.56	
Volumetric medium	α_a (in m^{-1})	X	5.00×10^{-3}	X	X
	β_a (in $\text{m}^{-1} \cdot \text{sr}^{-1}$)		7.14×10^{-5}		
	LR_a (in sr)		70		

Table 1. Input optical parameters of the scene used in the lidar simulator (PERFALIS code) as illustrated on Fig. 1

210 Inversion methods are generally applied to averaged signals in order to increase the SNR . In lidar remote sensing, the noise can be, approximately, considered as a white Gaussian noise (Li et al., 2012; Mao et al., 2013; Sun, 2018). In order to assess the impact of noise in the inversion method (see Section 3), a Gaussian noise of null mean value and a standard deviation of 1.5×10^{-5} a.u. is introduced in the theoretical lidar signals. Figure 3 displays the theoretical noised signals V_s and V_{sv} . As expected, because of light extinction by the plume, $V_{sv}(r_s)$ is lower than $V_s(r_s)$ by 9%. Four datasets are then generated, with
 215 respectively, an averaging over 20, 50, 100, and 200 signals, from V_s and V_{sv} , and, in addition, a fifth signal without noise is considered (Fig. 4).

¹PERFORMANCE Assessment for LIdar Systems

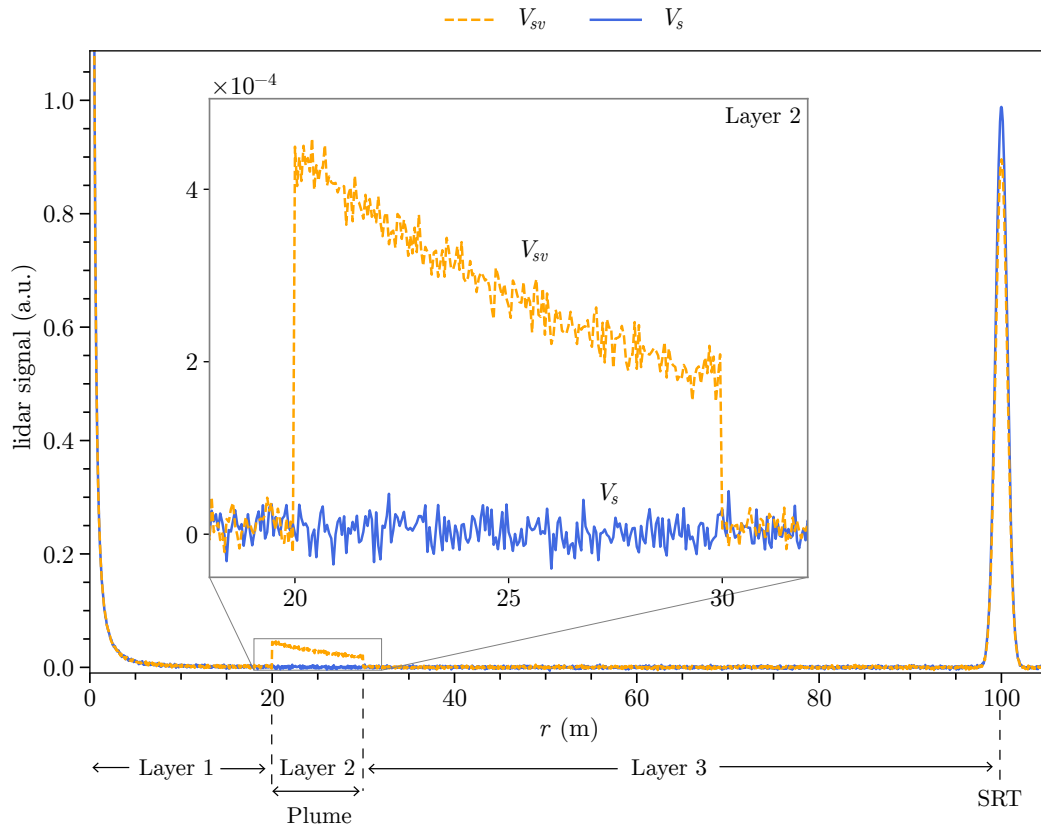


Figure 3. Theoretical noised lidar signals from a SRT V_s (blue line) and in the presence of an aerosol plume V_{sv} (orange dashed line). Simulations have been performed at 532 nm with molecular and continental aerosol background contributions.

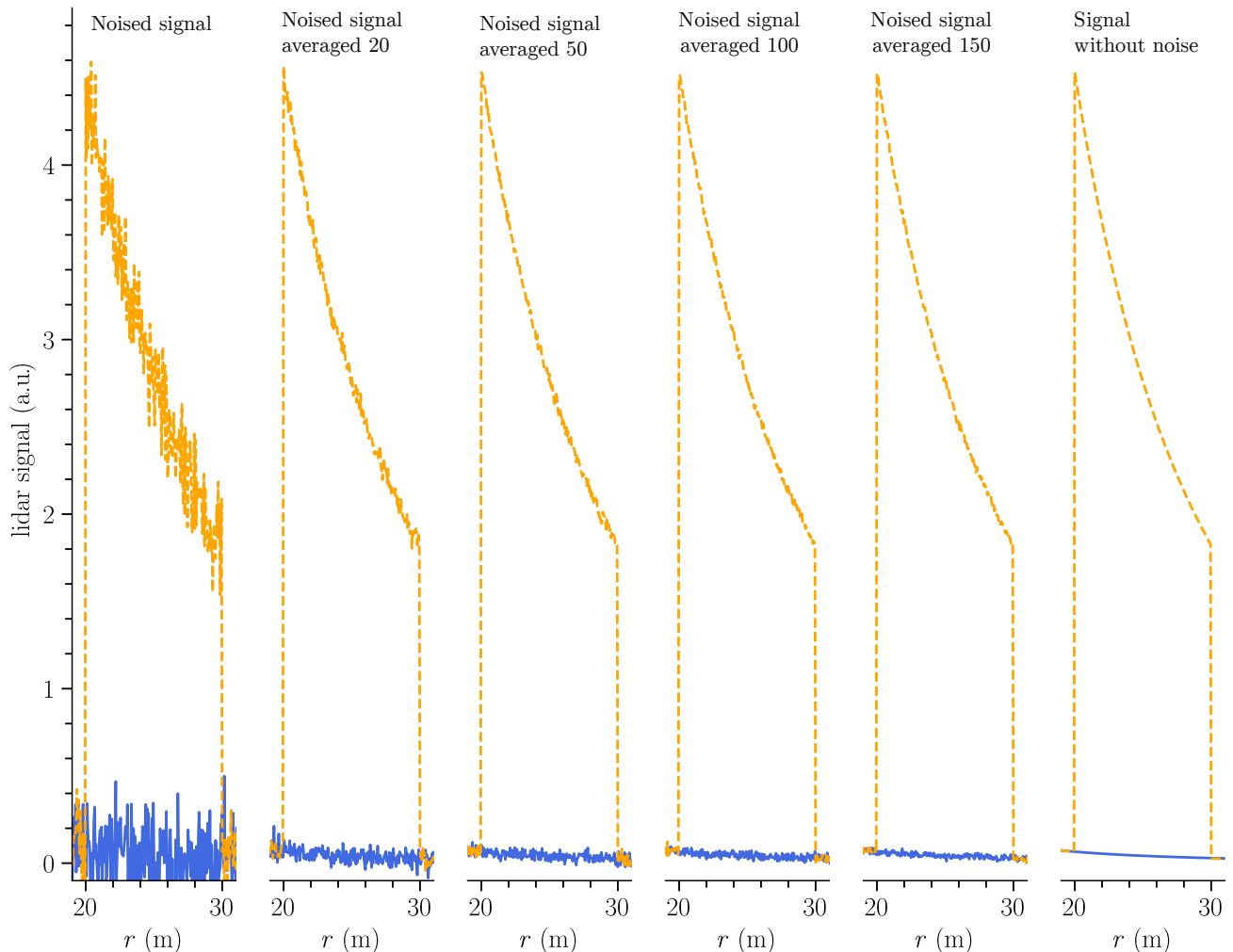


Figure 4. Lidar data sets used in the inversion method. In blue, (orange) the lidar signal in the absence (presence) of the volumetric media under study.

4.2 Noise impact on β_a and LR_a retrievals

LR_a is retrieved using Eq. 15. In addition to the six lidar-dataset described above, four different conditions of inversion are considered. In condition 1 the exact data of the background components are used as an input of the inversion algorithm. For conditions 2 and 3, β_b is over- and underestimated by 20% compared to the data used to generate the theoretical signals. In conditions 1 to 3, the inversion technique is performed over the entire signal range. Condition 4 is the same as condition 1, but the aerosol plume is spatially delimited. Table 2 summarizes the four-conditions for the six datasets. It is worth mentioning that

noised lidar signals obviously results in noised retrieved $\beta_a(r)$. Thus, to quantify the performance of the inversion technique, we consider the average value $\overline{\beta_a}$ of the plume. The retrieved value of LR_a can be directly compared to the theoretical value.

Conditions	1	2	3	4
Exact background constituents	X			X
$\beta_b + 20\%$		X		
$\beta_b - 20\%$			X	
Spatially bounded plume				X

Table 2. Conditions on the optical properties of the background components for the inversion method.

225 Figure 5 displays $\overline{\beta_a}$ for the six datasets and the four inversion conditions. It varies from 7.11×10^{-5} to $7.22 \times 10^{-5} \text{ m}^{-1} \cdot \text{sr}^{-1}$, which means an error of approximately 1% in comparison to the theoretical value. Conditions 2 and 3 result in a translation of the corresponding curve of $\pm 0.4\%$ with respect to the curve associated to condition 1, because of the over- and underestimation of 20% introduced in β_b . The performance is better for condition 4 whatever the dataset, since the maximum error is 0.5% for noised signals. The spatially bounded aerosol layer is often applied in inversion methods, and seem to herein improve the
 230 inversion method. For signal lidar without noise, $\overline{\beta_a}$ is not exactly equal to the theoretical value, maybe because of numerical computation errors in the inversion algorithm. Such a numerical error is about 0.12% (condition 1) and 0.04% (condition 4).

Fig. 6 is similar as Fig. 5 but considering LR_a . One obtains values ranging from 66 to 74sr, with a maximum error of 5% compared to the theoretical value. In conditions 1, 2, and 3, using averaged noised signals has no consequence on the retrieved value of LR_a , contrary to what was obtained for $\overline{\beta_a}$. In condition 1, the maximum error is 2.1%. The graphs corresponding
 235 to conditions 2 and 3 are translated, with respect to the graph under to condition 1, by about $\pm 3\%$, and permuted respectively to the same but for $\overline{\beta_a}$. Nevertheless, the errors remain low with a maximum of 5% (condition 2) if 50 signals are averaged. However, under condition 4, the LR_a is much better for averaged signals and remains quite good for noisy signal (not averaged) with an error rate of 0.6%. Again, it seems that the spatial limitation of the plume increases the accuracy of the retrieval LR_a . Condition 1 remains however efficient for noised signals since deviation is below 2.1%. In the case of lidar signal without
 240 noise, the retrieved LR_a are not exactly equal to the theoretical LR_a ; numerical computation errors are about 0.13% (condition 1) and 0.05% (condition 4). An error of $\pm 20\%$ on β_b introduced initially will result in an under- or overestimation LR_a by $\pm 3\%$. Condition 4 is preferable to retrieve LR_a .

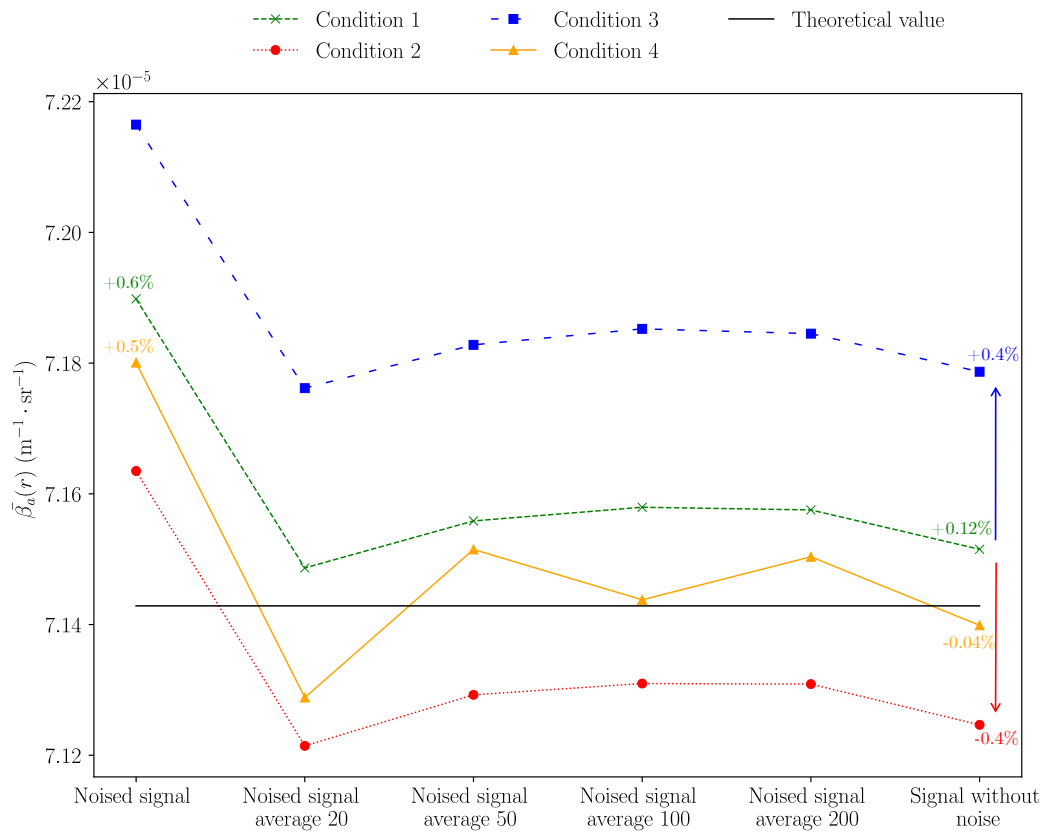


Figure 5. Retrieved $\bar{\beta}_a$ for six datasets and four different conditions of inversion.

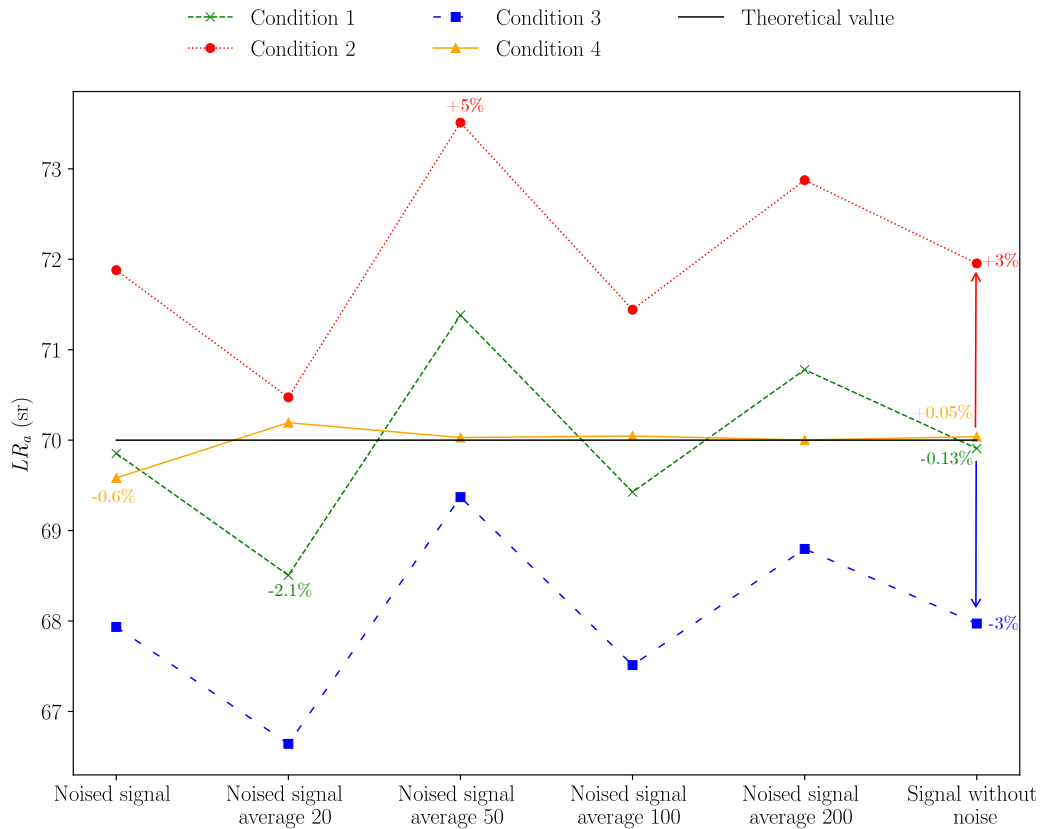


Figure 6. Retrieved LR_a for six datasets and four different conditions of inversion.

Note that the formalism and methodology adopted here to retrieve the lidar ratio are efficient as long as the peak backscattering of the SRT is present on the lidar signal. The method has been evaluated, in this manuscript, for short range around 100m because our research focus on application at this range. However, the algorithm developed does not present any limit with respect to the range provided that measurements are made below 1 km of range (this value depends of the power of laser sources) with respect to our applications. However, at first sight there is no limit to the application of the method to measurements at longer ranges such as more than 1 km measurements.

4.3 Plume optical property retrieval

The above study allowed us to test the new inversion method on noised signals, for different conditions of inversion, as a function of the number of signals averaged. Thereafter, lidar inversion is performed considering a spatially bounded plume and 100 signals for averaging. This last condition has been chosen because it corresponds to the number of signals available in less than 0.1 s with our lidar system (see Section 5). The theoretical results obtained by the inversion method with 100 averaged signals is also quite good (see above). Figure 9 displays the retrieved β_a if a theoretical lidar signal is introduced as a first

255 guess. Table 3 lists the retrieved $\bar{\beta}_a$ and LR_a . Compared to theoretical values, errors are less than 0.7% for LR_a and below 0.1% for $\bar{\beta}_a$, although a peak of 2.2% is observed at $r = 28.8$ m.

	LR_a	$\bar{\beta}_a$
Value	70.05 sr	$7.14 \times 10^{-5} \text{ m}^{-1} \cdot \text{sr}^{-1}$
Error	0.07%	0.01%

Table 3. Plume optical property retrieved and associated errors

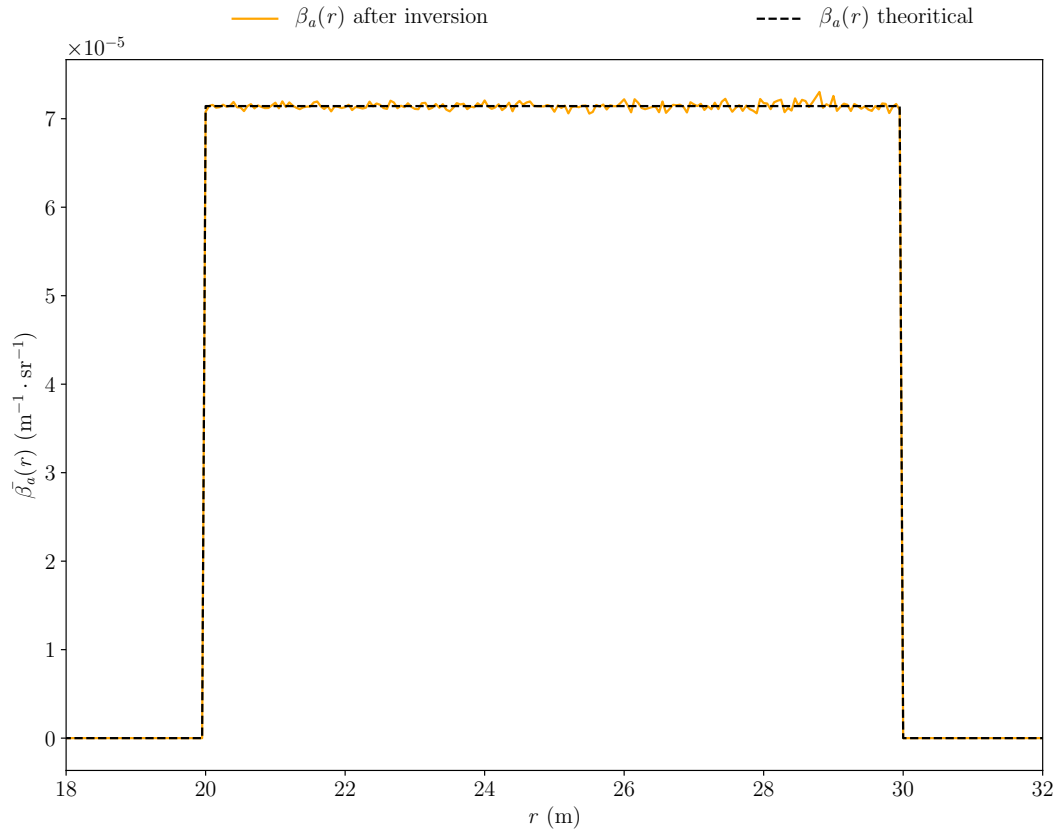


Figure 7. Retrieved $\beta_a(r)$ (orange solid line) for 100 theoretical averaged lidar signals and initial $\beta_a(r)$ (dark dashed line).

5 Case of real measurements

Our new inversion technique is now applied to real lidar measurements. The instrument used is named COLIBRIS² (Gaudfrin et al., 2018b)(Ceolato and Gaudfrin, 2018). This lidar is able to perform short-range measurements ($r_0 < 5$ m) at high spatial

²Compact lidar for Broadbord polaRIsation Spectral multi-Static measurement

260 resolution (lower than 0.25 m). A Nd:YAG microchip laser source of the HORUS-LEUKOS company is used with a pulse energy peaking at 532 nm of $7.3 \mu\text{J}$ and a repetition rate of 1 kHz. The backscattered light is collected by a Cassegrain telescope. In the detection part, a dichroic filter for the elastic channel is used before a photomultiplier tube. The signal is digitized at a sample frequency of 3 GHz after been amplified.

5.1 Description of the experimental operations

265 The lidar measurements are performed horizontally as illustrated in Fig. 8. A Lambertian Zenithal SRT (SphereOptic) with a $f_r = 0.20/\pi$ is placed at 52 m far away from the source. Its spectral bidirectional reflectance has been checked using laboratory bench measurements (Ceolato et al., 2012). The mean direction of the laser beam is parallel to the normal of the surface.

The repetition laser source has repetition frequency of 1 kHz. In order to increase the SNR , we preprocess the measurements from three lidar measurements:

- 270
- Signal 1. The first measurement is made by occulting the emitted laser beam to get a measure of the background scene (contribution of passive illumination);
 - Signal 2. The second measurement is made by occulting the telescope to estimate the dark noise of the instrument;
 - Signal 3. The last measurement is made without any occultation.

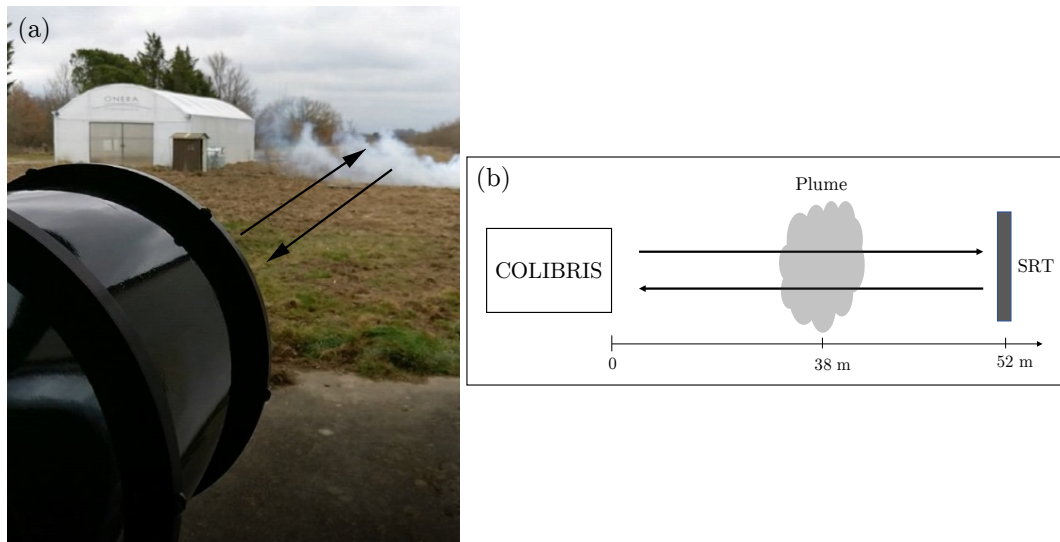


Figure 8. Experimental setup in an horizontal configuration. A fog-oil plume is generated between the lidar and the Lambertian SRT. (a) Photo and (b) illustration of the experimental setup with fog-oil plume.

For a given acquisition period, these three series of measured signals are averaged. The averaged signals of the background
275 radiation and the dark noise (signals 1 and 2) are then subtracted from the signal 3 such as : signal 3 - (signal 1 - signal 2).

Fig. 9 shows the lidar results on a volume/surface target over a period of 2s. This corresponds to 2000 signals per serie of measurements. During this period, we assume that the environment does not evolve significantly. The curves V_{sv} and V_s are the measurements in the presence and in the absence of oil smoke with SRT, respectively. The oil plume signal is visible between 37.5m and 41 m.

280 The high-speed sampling allows a measurement every 5 cm along the line of sight. Combined with a short pulse duration of the laser source (1.7 ns), this makes it possible to highlight local variations concentration in the order of 25 cm inside the plume with the presence of two maxima at 38m and 39m from lidar. The peak of backscattering of the SRT is also well sampled. The signal amplitude corresponding to the backscatter of the SRT is lower on V_{sv} than on V_s because of the presence of the oil plume.

285 During measurement, the pressure, temperature and visibility are respectively 1016hPa, 288K and 30km. These data are used to compute β_b as described in Section 4.

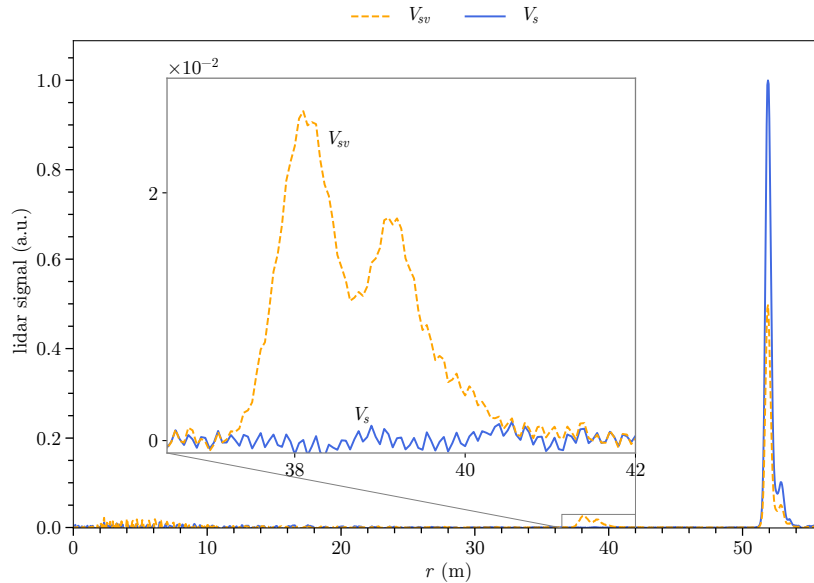


Figure 9. Lidar measurements of the experimental setup. In blue, (orange) the lidar signal in the absence (presence) of the oil-fog plume under study.

5.2 Optical property retrieval: fog-oil plume

The signals V_s and V_{sv} are used in the inversion procedure as described in Sections 3 and 4. The plume is spatially bounded (condition 4). The retrieved $\beta_a(r)$ is displayed in Fig. 10. In the densest range of the plume $\beta_a \approx 2 \times 10^{-3} \text{ m}^{-1} \text{ sr}^{-1}$. Also, the

290 retrieved LR_a is around 98sr. According to Bohlmann et al. (2018), this value corresponds, as expected, to smoke particles (at 532nm, the lidar ratio ranges from 80 to 100sr). The optical properties of the oil-fog plume of experimental retrieved with inverse method are summarized in Section 4.

The lidar signal reproduced from the retrieved $\beta_a(r)$, LR_a and of the instrumental constant deduced from the Eq. 14 gives a standard deviation from the exact value of 1.5×10^{-5} a.u. This shows the consistency and reliability of the new inversion
 295 method proposed in this paper.

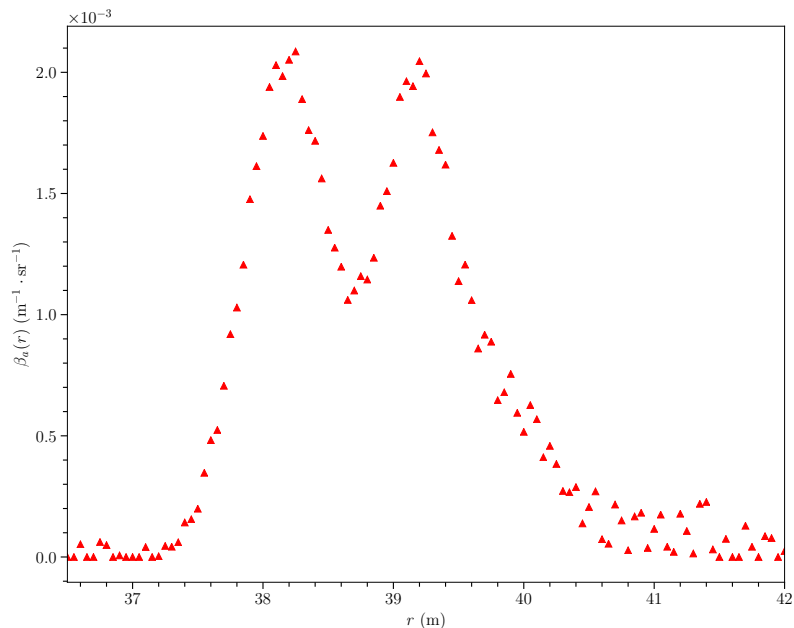


Figure 10. Retrieved $\beta_a(r)$ for real measurements with $LR_a = 98$ sr.

LR_a (sr)	98
$\beta_{a,max}$ ($\text{m}^{-1} \cdot \text{sr}^{-1}$)	2.1×10^{-3}
$\alpha_{a,max}$ (m^{-1})	2.1×10^{-1}
Optical thickness	3.6×10^{-1}

Table 4. Optical properties of oil-fog plume in experimental setup at 532nm

6 Conclusions

In this paper, a new method has been introduced for lidar measurement inversion in a situation for which a volumetric layer (molecular Rayleigh scatterers) of the high troposphere is not available (e.g. airborne lidar observations, horizontal configuration of measurements). This method is based on a new expression of the lidar equation which allows us to use a surface

300 reference target of a known BRDF instead of a volumetric one. This new formalism permits to invert short-range lidar measurements for which conventional inversion techniques can not directly be applied. Similarly to common inversion techniques, our method requires to introduce a background component (molecular and particulate contributions) that can be estimated either from radiative models or deduced from measurements of temperature, pressure, and visibility conditions.

Also, a new algorithm has been developed to retrieve, without any *a priori* assumptions relative to the medium to be characterized (aerosol plume), the backscattering coefficient (β_a) and lidar ratio (LR_a) of an aerosol plume, between the lidar and the surface target reference. In other words, our technique method does not need to introduce any lidar ratio as an input for our inverse algorithm. For that, two lidar measurements are necessary: with and without the aerosol plume under consideration. Comparing these two signals, one can retrieve the total extinction coefficient of the medium analysed and the instrumental constant of the lidar instrument. These two informations are used to constrain the inversion algorithm and finally to identify
310 LR_a .

This algorithm has been first investigated using theoretical (simulated) lidar signals. The quality of the retrieval has been assessed by introducing noise in the simulated signals and by considering various conditions of inversion differing, in particular, from one another according to the initial error introduced in the backscattering coefficient of the aerosol background. Thus, the robustness of algorithm has been shown, since in all the cases, the error on the retrieved values (*viz.* in β_a and LR_a) is less
315 than 5%, at most. Also, we have found that inversion is better for spatially bounded aerosol plume.

The inversion algorithm has then been applied on real lidar short-range measurements of an oil-fog plume. The retrieved β_a and LR_a of the plume agree with values found in the literature for smoke-like particles. Moreover, thanks to the determination of the instrumental constant, the measured signal has been computed from the inverted products, and an absolute error of 10^{-5} between the measure and the post-processed simulation has been encountered.

320 However, it is worth mentioning that the method proposed herein to find LR_a has some limitations. Precisely, the sensitivity of the lidar must be sufficient to detect the signal of weakly thick or weakly backscattering plume.

Indeed, since measurements are performed in the absence and in the presence of the medium, by means of a hard surface target of reference of known reflectance, the algorithm converges less easily for very weakly diffusing plumes.

The new inversion technique presented in this paper suggests new airborne lidar applications operated at low altitude from
325 aircraft (helicopters, airplanes), but requires *a priori* knowledge of the reflectance of the SRT. Even if some models exist for the BRDF of surfaces (Bréon et al., 2002; Lobell and Asner, 2002; Mishchenko et al., 1999), their use seems difficult to implement because of the diversity of encountered surfaces during airborne measurements. Nevertheless, it may be possible to identify the reflectance of the ground surface by means of a spectroradiometer imager (Poutier et al., 2002; Miesch et al., 2005; Josset et al., 2018). The combination of these measurements with the herein proposed inversion method would be *a*
330 *priori* be complementary to establish new methods of calibration for downlooking lidar measurements (spaceborne or airborne lidars). The evaluation of the method proposed in this paper, considering the uncertainty of the target reflectance, has not been performed. It will be the topic of future works.

7 Appendix

To solve Eq. 9, the exponential term can be written under another form. The method proposed by Vande Hey (2014) consists in integrating both members of the equation from r to r_s . So:

$$\int_r^{r_s} W(x) dx = \frac{c\tau}{2f_r F_{cor}} \frac{W(r_s)}{LR_a(r_s)} \int_r^{r_s} \left\{ Y(x) \exp \left[2 \int_x^{r_s} Y(r) dr \right] \right\} dx$$

Since:

$$\begin{aligned} 335 \quad \frac{d}{dx} \left\{ \exp \left[2 \int_x^{r_s} Y(r) dr \right] \right\} &= 2 \exp \left[2 \int_x^{r_s} Y(r) dr \right] \frac{d}{dx} \left[\int_x^{r_s} Y(r) dr \right] \\ &= 2 \exp \left[2 \int_x^{r_s} Y(r) dr \right] \frac{d}{dx} [F(r_s) - F(x)] \\ &= -2Y(x) \exp \left[2 \int_x^{r_s} Y(r) dr \right] \end{aligned}$$

where F is the primitive of Y , it ensues:

$$\begin{aligned} 340 \quad \int_r^{r_s} Y(x) \exp \left[2 \int_x^{r_s} Y(r) dr \right] dx &= -\frac{1}{2} \left\{ \exp \left[2 \int_x^{r_s} Y(r) dr \right] \right\}_r^{r_s} \\ &= \frac{1}{2} \left\{ \exp \left[2 \int_r^{r_s} Y(r) dr \right] - 1 \right\} \end{aligned}$$

Therefore:

$$\int_r^{r_s} W(x) dx = \frac{c\tau}{4f_r F_{cor}} \frac{W(r_s)}{LR_a(r_s)} \left\{ \exp \left[2 \int_r^{r_s} Y(r) dr \right] - 1 \right\}$$

Finally, the exponential term becomes:

$$\exp \left[2 \int_r^{r_s} Y(r) dr \right] = 1 + \frac{4f_r F_{cor}}{c\tau} \frac{LR_a(r_s)}{W(r_s)} \left[\int_r^{r_s} W(r) dr \right]$$

Competing interests. The authors declare that they have no conflict of interest.

Acknowledgements. This research work has been performed within the framework of a CIFRE grant (ANRT) for the doctoral work of Florian Gaudfrin. The lidar systems has been funded by the PROMETE project (ONERA). The laser source used in this paper for the experimental setup has been designed by Benoit Faure, Paul-Henri Pioger, and Guillaume Huss from the company HORUS-LEUKOS.

345 **References**

- Estimates of the direct and indirect radiative forcing due to tropospheric aerosols: A review, *Reviews of Geophysics*, 38, 513–543, <https://doi.org/10.1029/1999RG000078>, 2000.
- Journal of Geophysical Research D: Atmospheres, 110, 1–13, <https://doi.org/10.1029/2004JD005124>, 2005.
- Combined Determination of the Chemical Composition and of Health Effects of Secondary Organic Aerosols: The POLYSOA Project, 350 *Journal of Aerosol Medicine and Pulmonary Drug Delivery*, 21, 145–154, <https://doi.org/10.1089/jamp.2007.0655>, 2008.
- Ackermann, J.: The extinction-to-backscatter ratio of tropospheric aerosol: A numerical study, *Journal of Atmospheric and Oceanic Technology*, 15, 1043–1050, [https://doi.org/10.1175/1520-0426\(1998\)015<1043:TETBRO>2.0.CO;2](https://doi.org/10.1175/1520-0426(1998)015<1043:TETBRO>2.0.CO;2), 1998.
- Anon: U.S. Standard Atmosphere, Tech. rep., NASA, Washington, DC, United States, 1976.
- Ansmann, A., Riebesell, M., and Weitkamp, C.: Measurement of atmospheric aerosol extinction profiles with a Raman lidar, *Optics Letters*, 355 15, 746, <https://doi.org/10.1364/OL.15.000746>, 1990.
- Ansmann, A., Wandinger, U., Riebesell, M., Weitkamp, C., and Michaelis, W.: Independent measurement of extinction and backscatter profiles in cirrus clouds by using a combined Raman elastic-backscatter lidar, *Applied Optics*, 31, 7113, <https://doi.org/10.1364/AO.31.007113>, 1992.
- Ansmann, A., Neuber, R., Rairoux, P., and Wandinger, U.: *Advances in Atmospheric Remote Sensing with Lidar*, vol. 34, Springer Berlin Heidelberg, Berlin, Heidelberg, <https://doi.org/10.1007/978-3-642-60612-0>, 1997.
- Ansmann, A., Baldasano, J., Calpini, B., Chaikovsky, Anatoly and Flamant, P., Mitev, V., Papayannis, A., Pelon, J., Resendes, D., Schneider, J., Trickl, T., and Vaughan, G.: EARLINET: A European Aerosol Research Lidar Network, Tech. rep., 2001.
- Berk, A., Acharya, P., and Bernstein, L.: Band model method for modeling atmospheric propagation at arbitrarily fine spectral resolution, 2008.
- 365 Berk, A., Conforti, P., Kennett, R., Perkins, T., Hawes, F., and van den Bosch, J.: MODTRAN6: a major upgrade of the MODTRAN radiative transfer code, vol. 9088, p. 90880H, International Society for Optics and Photonics, <https://doi.org/10.1117/12.2050433>, 2014.
- Bissonnette, L. R.: Multiple-scattering lidar equation, *Applied Optics*, 35, 6449, <https://doi.org/10.1364/AO.35.006449>, 1996.
- Bodhaine, B. A., Wood, N. B., Dutton, E. G., and Slusser, J. R.: On Rayleigh Optical Depth Calculations, *Journal of Atmospheric and Oceanic Technology*, 16, 1854–1861, [https://doi.org/10.1175/1520-0426\(1999\)016<1854:ORODC>2.0.CO;2](https://doi.org/10.1175/1520-0426(1999)016<1854:ORODC>2.0.CO;2), 1999.
- 370 Bohlmann, S., Baars, H., Radenz, M., Engelmann, R., and Macke, A.: *Atmospheric Chemistry and Physics*, 18, 9661–9679, <https://doi.org/10.5194/acp-18-9661-2018>, 2018.
- Bréon, F.-M., Maignan, F., Leroy, M., and Grant, I.: Analysis of hot spot directional signatures measured from space, *Journal of Geophysical Research*, 107, 4282, <https://doi.org/10.1029/2001JD001094>, 2002.
- Bucholtz, A.: Rayleigh-scattering calculations for the terrestrial atmosphere, *Applied Optics*, 34, 2765, 375 <https://doi.org/10.1364/AO.34.002765>, 1995.
- Bufton, J. L.: Laser Altimetry Measurements from Aircraft and Spacecraft, *Proceedings of the IEEE*, 77, 463–477, <https://doi.org/10.1109/5.24131>, 1989.
- Ceolato, R. and Gaudfrin, F.: Short-range characterization of freshly emitted carbonaceous particles by LiDAR, in: General Meeting, Nafplio, 2018.
- 380 Ceolato, R., Riviere, N., and Hespel, L.: Reflectances from a supercontinuum laser-based instrument: hyperspectral, polarimetric and angular measurements, *Optics Express*, 20, 29 413, <https://doi.org/10.1364/oe.20.029413>, 2012.

- Ceolato, R., Gaudfrin, F., Pujol, O., Riviere, N., Berg, M. J., and Sorensen, C. M.: Lidar cross-sections of soot fractal aggregates: Assessment of equivalent-sphere models, *Journal of Quantitative Spectroscopy and Radiative Transfer*, 212, 39–44, <https://doi.org/10.1016/j.jqsrt.2017.12.004>, 2018.
- 385 Clark, W. E. and Whitby, K. T.: Concentration and Size Distribution Measurements of Atmospheric Aerosols and a Test of the Theory of Self-Preserving Size Distributions, *Journal of the Atmospheric Sciences*, 24, 677–687, [https://doi.org/10.1175/1520-0469\(1967\)024<0677:CASDMO>2.0.CO;2](https://doi.org/10.1175/1520-0469(1967)024<0677:CASDMO>2.0.CO;2), 1967.
- Collis, R. T. H. and Russell, P. B.: Lidar measurement of particles and gases by elastic backscattering and differential absorption, pp. 71–151, https://doi.org/10.1007/3-540-07743-X_18, 1976.
- 390 Comeron, A., Sicard, M., Kumar, D., and Rocadenbosch, F.: Use of a field lens for improving the overlap function of a lidar system employing an optical fiber in the receiver assembly, *Applied Optics*, 50, 5538, <https://doi.org/10.1364/AO.50.005538>, 2011.
- Dawson, K. W., Meskhidze, N., Josset, D., and Gassó, S.: Spaceborne observations of the lidar ratio of marine aerosols, *Atmospheric Chemistry and Physics*, 15, 3241–3255, <https://doi.org/10.5194/acp-15-3241-2015>, 2015.
- DeMott, P. J., Prenni, A. J., Liu, X., Kreidenweis, S. M., Petters, M. D., Twohy, C. H., Richardson, M. S., Eidhammer, T., and Rogers, D. C.: Predicting global atmospheric ice nuclei distributions and their impacts on climate, *Proceedings of the National Academy of Sciences*, 107, 11 217–11 222, <https://doi.org/10.1073/pnas.0910818107>, 2010.
- Elias, T., Haeffelin, M., Drobinski, P., Gomes, L., Rangognio, J., Bergot, T., Chazette, P., Raut, J. C., and Colomb, M.: Particulate contribution to extinction of visible radiation: Pollution, haze, and fog, *Atmospheric Research*, 92, 443–454, <https://doi.org/10.1016/j.atmosres.2009.01.006>, 2009.
- 400 Fernald, F. G.: Analysis of atmospheric lidar observations: some comments, *Applied Optics*, 23, 652, <https://doi.org/10.1364/ao.23.000652>, 1984.
- Fernald, F. G., Herman, B. M., and Reagan, J. A.: Determination of Aerosol Height Distributions by Lidar, *Journal of Applied Meteorology*, 11, 482–489, [https://doi.org/10.1175/1520-0450\(1972\)011<0482:DOAHDB>2.0.CO;2](https://doi.org/10.1175/1520-0450(1972)011<0482:DOAHDB>2.0.CO;2), 1972.
- Finlayson-Pitts, B. J. and Pitts, J. N. J.: The Atmospheric System, *Chemistry of the Upper and Lower Atmosphere: Theory, Experiments, and Applications*, pp. 15–42, <https://doi.org/10.1016/B978-012257060-5/50004-6>, 2000.
- 405 Gaudfrin, F., Ceolato, R., Pujol, O., Riviere, N., and Hu, Q.: Supercontinuum lidar for hydrometeors and aerosols optical properties determination, in: EGU General Assembly 2018, vol. 20, p. 14436, 2018a.
- Gaudfrin, F., Ceolato, R., Riviere, N., Pujol, O., and Huss, G.: New technics to probe aerosols radiative properties from visible to infrared, in: *The 13th International IR Target and Background Modeling & Simulation Workshop*, Banyuls-sur-Mer, 2018b.
- 410 Gaudfrin, F., Ceolato, R., Pujol, O., and Riviere, N.: A new-lidar inversion technique using a surface reference target at short - range, in: *The 29th International Laser Radar Conference*, pp. 3–6, Hefei, 2019.
- Getzewich, B. J., Vaughan, M. A., Hunt, W. H., Avery, M. A., Powell, K. A., Tackett, J. L., Winker, D. M., Kar, J., Lee, K.-P., and Toth, T. D.: CALIPSO lidar calibration at 532 nm: version 4 daytime algorithm, *Atmospheric Measurement Techniques*, 11, 6309–6326, <https://doi.org/10.5194/amt-11-6309-2018>, <https://www.atmos-meas-tech.net/11/6309/2018/>, 2018.
- 415 Glickman, T. and Zenk, W.: *Glossary of Meteorology*, American Meteorological Society, Boston, 855 pp. 2, 2000.
- Hadamard, J.: Théorie des équations aux dérivées partielles linéaires hyperboliques et du problème de Cauchy, *Acta Mathematica*, 31, 333–380, <https://doi.org/10.1007/BF02415449>, 1908.
- Hall, F. F. and Ageo, H. Y.: Absolute calibration of a laser system for atmospheric probing, *Applied Optics*, 9, 1820–1824, <https://doi.org/10.1364/AO.9.001820>, 1970.

- 420 Halldórsson, T. and Langerholc, J.: Geometrical form factors for the lidar function, *Applied Optics*, 17, 240, <https://doi.org/10.1364/AO.17.000240>, 1978.
- Haner, D. A., McGuckin, B. T., Menzies, R. T., Bruegge, C. J., and Duval, V.: Directional-hemispherical reflectance for Spectralon by integration of its bidirectional reflectance, *Applied Optics*, 37, 3996, <https://doi.org/10.1364/AO.37.003996>, 1998.
- Hansen, J., Sato, M., and Ruedy, R.: Radiative forcing and climate response, *Journal of Geophysical Research: Atmospheres*, 102, 6831–425 6864, <https://doi.org/10.1029/96JD03436>, 1997.
- Hess, M., Koepke, P., Schult, I., Hess, M., Koepke, P., and Schult, I.: Optical Properties of Aerosols and Clouds: The Software Package OPAC, *Bulletin of the American Meteorological Society*, 79, 831–844, [https://doi.org/10.1175/1520-0477\(1998\)079<0831:OPOAAC>2.0.CO;2](https://doi.org/10.1175/1520-0477(1998)079<0831:OPOAAC>2.0.CO;2), 1998.
- Hoff, R. M., Bösenberg, J., and Pappalardo, G.: The GAW Aerosol Lidar Observation Network (GALION), in: *International Geoscience and Remote Sensing Symposium (IGARSS-08)*, Boston (USA), pp. 6–11, 2008.
- 430 Horvath, H.: On the applicability of the Koschmieder visibility formula, 5, 177–184, [https://doi.org/10.1016/0004-6981\(71\)90081-3](https://doi.org/10.1016/0004-6981(71)90081-3), 1971.
- Hu, Y., Vaughan, M., Liu, Z., Powell, K., and Rodier, S.: Retrieving Optical Depths and Lidar Ratios for Transparent Layers Above Opaque Water Clouds From CALIPSO Lidar Measurements, *IEEE Geoscience and Remote Sensing Letters*, 4, 523–526, <https://doi.org/10.1109/LGRS.2007.901085>, 2007.
- 435 Hyslop, N. P.: Impaired visibility: the air pollution people see, *Atmospheric Environment*, 43, 182–195, <https://doi.org/10.1016/j.atmosenv.2008.09.067>, 2009.
- Jäger, H.: Long-term record of lidar observations of the stratospheric aerosol layer at Garmisch-Partenkirchen, *Journal of Geophysical Research D: Atmospheres*, 110, 1–9, <https://doi.org/10.1029/2004JD005506>, 2005.
- Josset, D., Pelon, J., Protat, A., and Flamant, C.: New approach to determine aerosol optical depth from combined CALIPSO and CloudSat 440 ocean surface echoes, *Geophysical Research Letters*, 35, <https://doi.org/10.1029/2008GL033442>, 2008.
- Josset, D., Pelon, J., and Hu, Y.: Multi-Instrument Calibration Method Based on a Multiwavelength Ocean Surface Model, *IEEE Geoscience and Remote Sensing Letters*, 7, 195–199, <https://doi.org/10.1109/LGRS.2009.2030906>, <http://ieeexplore.ieee.org/document/5299031/>, 2010a.
- Josset, D., Zhai, P.-W., Hu, Y., Pelon, J., and Lucker, P. L.: Lidar equation for ocean surface and subsurface, *Optics Express*, 18, 20 862, 445 <https://doi.org/10.1364/OE.18.020862>, 2010b.
- Josset, D., Pelon, J., Garnier, A., Hu, Y., Vaughan, M., Zhai, P.-W., Kuehn, R., and Lucker, P.: Cirrus optical depth and lidar ratio retrieval from combined CALIPSO-CloudSat observations using ocean surface echo, *Journal of Geophysical Research: Atmospheres*, 117, n/a–n/a, <https://doi.org/10.1029/2011jd016959>, 2012.
- Josset, D., Pelon, J., Pascal, N., Hu, Y., and Hou, W.: On the Use of CALIPSO Land Surface Returns to Retrieve Aerosol and Cloud Optical 450 Depths, *IEEE Transactions on Geoscience and Remote Sensing*, 56, 3256–3264, <https://doi.org/10.1109/TGRS.2018.2796850>, 2018.
- Kar, J., Vaughan, M. A., Lee, K.-P., Tackett, J. L., Avery, M. A., Garnier, A., Getzewich, B. J., Hunt, W. H., Josset, D., Liu, Z., Lucker, P. L., Magill, B., Omar, A. H., Pelon, J., Rogers, R. R., Toth, T. D., Trepte, C. R., Vernier, J.-P., Winker, D. M., and Young, S. A.: CALIPSO lidar calibration at 532 nm: version 4 nighttime algorithm, *Atmospheric Measurement Techniques*, 11, 1459–1479, <https://doi.org/10.5194/amt-11-1459-2018>, <https://www.atmos-meas-tech.net/11/1459/2018/>, 2018.
- 455 Kavaya, M. J., Menzies, R. T., Haner, D. A., Oppenheim, U. P., and Flamant, P. H.: Target reflectance measurements for calibration of lidar atmospheric backscatter data, *Applied Optics*, 22, 2619, <https://doi.org/10.1364/AO.22.002619>, 1983.

- Klett, J. D.: Stable analytical inversion solution for processing lidar returns, *Applied Optics*, 20, 211, <https://doi.org/10.1364/AO.20.000211>, 1981.
- Klett, J. D.: Lidar inversion with variable backscatter/extinction ratios, *Applied Optics*, 24, 1638, <https://doi.org/10.1364/AO.24.001638>, 1985.
- 460 Kraft, D.: Software Package for Sequential Quadratic Programming, 1988.
- Kumar, D. and Rocadenbosch, F.: Determination of the overlap factor and its enhancement for medium-size tropospheric lidar systems: a ray-tracing approach, *Journal of Applied Remote Sensing*, 7, 073591, <https://doi.org/10.1117/1.JRS.7.073591>, 2013.
- Labarre, L., Caillaud, K., Fauqueux, S., Malherbe, C., Roblin, A., Rosier, B., and Simoneau, P.: An overview of MATISSE-v2.0, p. 782802, <https://doi.org/10.1117/12.868183>, 2010.
- 465 Leblanc, T., Trickl, T., and Vogelmann, H.: Lidar, vol. 102 of *Springer Series in Optical Sciences*, Springer-Verlag, New York, <https://doi.org/10.1007/b106786>, 2005.
- Li, J., Gong, W., and Ma, Y.: Atmospheric Lidar Noise Reduction Based on Ensemble Empirical Mode Decomposition, ISPRS - International Archives of the Photogrammetry, Remote Sensing and Spatial Information Sciences, XXXIX-B8, 127–129, <https://doi.org/10.5194/isprsarchives-XXXIX-B8-127-2012>, 2012.
- 470 Lobell, D. B. and Asner, G. P.: Moisture Effects on Soil Reflectance, *Soil Science Society of America Journal*, 66, 722, <https://doi.org/10.2136/sssaj2002.7220>, 2002.
- Mao, F., Gong, W., and Li, C.: Anti-noise algorithm of lidar data retrieval by combining the ensemble Kalman filter and the Fernald method, *Optics Express*, 21, 8286, <https://doi.org/10.1364/OE.21.008286>, 2013.
- 475 Matsumoto, M. and Takeuchi, N.: Effects of misestimated far-end boundary values on two common lidar inversion solutions, *Applied Optics*, 33, 6451, <https://doi.org/10.1364/AO.33.006451>, 1994.
- Mattis, I., Ansmann, A., Müller, D., Wandinger, U., and Althausen, D.: Multilayer aerosol observations with dual-wavelength Raman lidar in the framework of EARLINET, *Journal of Geophysical Research D: Atmospheres*, 109, 1–15, <https://doi.org/10.1029/2004JD004600>, 2004.
- 480 Measures, R. M.: *Laser Remote Sensing: Fundamentals and Applications*, reprint ed edn., <http://doi.wiley.com/10.1029/EO066i040p00686-05>, 1992.
- Miesch, C., Poutier, L., Achard, V., Briottet, X., Lenot, X., and Boucher, Y.: Direct and inverse radiative transfer solutions for visible and near-infrared hyperspectral imagery, *IEEE Transactions on Geoscience and Remote Sensing*, 43, 1552–1562, <https://doi.org/10.1109/TGRS.2005.847793>, 2005.
- 485 Mishchenko, M. I., Dlugach, J. M., Yanovitskij, E. G., and Zakharova, N. T.: Bidirectional reflectance of flat, optically thick particulate layers: an efficient radiative transfer solution and applications to snow and soil surfaces, *Journal of Quantitative Spectroscopy and Radiative Transfer*, 63, 409–432, [https://doi.org/10.1016/S0022-4073\(99\)00028-X](https://doi.org/10.1016/S0022-4073(99)00028-X), 1999.
- Nicodemus, F. E.: Directional Reflectance and Emissivity of an Opaque Surface, *Applied Optics*, 4, 767, <https://doi.org/10.1364/AO.4.000767>, 1965.
- 490 O'Connor, E. J., Illingworth, A. J., and Hogan, R. J.: A Technique for Autocalibration of Cloud Lidar, *Journal of Atmospheric and Oceanic Technology*, 21, 777–786, 2004.
- Painemal, D., Clayton, M., Ferrare, R., Burton, S., Josset, D., and Vaughan, M.: Novel aerosol extinction coefficients and lidar ratios over the ocean from CALIPSO–CloudSat: evaluation and global statistics, *Atmospheric Measurement Techniques*, 12, 2201–2217, <https://doi.org/10.5194/amt-12-2201-2019>, 2019.

- 495 Paschotta, R.: Field Guide to Laser Pulse Generation, vol. FG14, <https://doi.org/10.1111/j.1749-6632.1965.tb20241.x>, 2008.
- Pedros, R., Estellés, V., Sicard, M., Gómez-Amo, J. L., Utrillas, M. P., Martínez-Lozano, J. A., Rocadenbosch, F., Pérez, C., and Recio Baldasano, J. M.: Climatology of the aerosol extinction-to-backscatter ratio from sun-photometric measurements, *IEEE Transactions on Geoscience and Remote Sensing*, 48, 237–249, <https://doi.org/10.1109/TGRS.2009.2027699>, 2010.
- Popovicheva, O. B., Engling, G., Ku, I.-T., Timofeev, M. A., and Shonija, N. K.: Aerosol Emissions from Long-Lasting Smoldering of Boreal Peatlands: Chemical Composition, Markers, and Microstructure, *Aerosol and Air Quality Research*, 2, 213–218, <https://doi.org/10.4209/aaqr.2018.08.0302>, 2019.
- 500 Poutier, L., Miesch, C., Lenot, X., Achard, V., and Boucher, Y.: COMANCHE and COCHISE: two reciprocal atmospheric codes for hyperspectral remote sensing, Tech. rep., http://www.onecert.fr/pirrene/references/{_}docs/poutier{_{_}et{_{_}al{_{_}AVIRIS{_{_}2002.pdf, 2002.
- Rocadenbosch, F., Frasier, S., Kumar, D., Lange Vega, D., Gregorio, E., and Sicard, M.: Backscatter error bounds for the elastic lidar two-component inversion algorithm, *IEEE Transactions on Geoscience and Remote Sensing*, 50, 4791–4803, <https://doi.org/10.1109/TGRS.2012.2194501>, 2012.
- 505 Sasano, Y., Browell, E. V., and Ismail, S.: Error caused by using a constant extinction/backscattering ratio in the lidar solution, *Applied Optics*, 24, 3929, <https://doi.org/10.1364/AO.24.003929>, 1985.
- Sicard, M., Chazette, P., Pelon, J., Won, J., and Yoon, S.-C.: Variational method for the retrieval of the optical thickness and the backscatter coefficient from multiangle lidar profiles, *Applied Optics*, 41, 493–502, <https://doi.org/10.1364/AO.41.000493>, 2002.
- 510 Simoneau, P., Berton, R., Caillault, K., Durand, G., Huet, T., Labarre, L., Malherbe, C., Miesch, C., Roblin, A., and Rosier, B.: MATISSE: advanced Earth modeling for imaging and scene simulation, in: *Proceedings of SPIE*, edited by Kohnle, A., Gonglewski, J. D., and Schmutge, T. J., vol. 4538, p. 39, <https://doi.org/10.1117/12.454410>, 2002.
- SphereOptic: Diffusers, Zenith Polymer, Foil, nearly ideal Lambertian > SphereOptics EN, <https://sphereoptics.de/en/product/zenith-polymer-diffusers/?c=79>.
- 515 Stelmaszczyk, K., Dell’Aglia, M., Chudzyński, S., Stacewicz, T., and Wöste, L.: Analytical function for lidar geometrical compression form-factor calculations, *Applied Optics*, 44, 1323, <https://doi.org/10.1364/AO.44.001323>, 2005.
- Sun, X.: *Lidar Sensors From Space*, Elsevier, <https://doi.org/10.1016/B978-0-12-409548-9.10327-6>, 2018.
- Swinehart, D.: The Beer-Lambert law, *Journal of Chemical Education*, 39, 335, <https://doi.org/10.1021/ed039p333>, 1962.
- 520 Vande Hey, J., Coupland, J., Foo, M. H., Richards, J., and Sandford, A.: Determination of overlap in lidar systems, *Applied Optics*, 50, 5791, <https://doi.org/10.1364/AO.50.005791>, 2011.
- Vande Hey, J. D.: Theory of Lidar, pp. 23–41, https://doi.org/10.1007/978-3-319-12613-5_2, 2014.
- Vargas-Ubera, J., Aguilar, J. F., and Gale, D. M.: Reconstruction of particle-size distributions from light-scattering patterns using three inversion methods, *Applied Optics*, 46, 124, <https://doi.org/10.1364/AO.46.000124>, 2007.
- 525 Wandinger, U. and Ansmann, A.: Experimental determination of the lidar overlap profile with Raman lidar, *Applied Optics*, 41, 511–514, <https://doi.org/10.1364/AO.41.000511>, 2002.
- Young, S. A.: Analysis of lidar backscatter profiles in optically thin clouds, *Appl. Opt.*, 34, 7019–7031, <https://doi.org/10.1364/AO.34.007019>, <http://ao.osa.org/abstract.cfm?URI=ao-34-30-7019>, 1995.
- Zhang, J., Wei, E., Wu, L., Fang, X., Li, F., Yang, Z., Wang, T., and Mao, H.: Elemental Composition and Health Risk Assessment of PM10 and PM2.5 in the Roadside Microenvironment in Tianjin, China, *Aerosol and Air Quality Research*, 18, 1817–1827, <https://doi.org/10.4209/aaqr.2017.10.0383>, 2018.
- 530